

# Filtration-Based Representation Learning for Temporal Graphs

**Samrik Chowdhury**

Indian Institute of Science Education and Research Tirupati, India.

**Siddharth Pritam** ✉

Chennai Mathematical Institute, India.

**Rohit Roy**

Chennai Mathematical Institute, India.

**Madhav Cherupilil Sajeev**

Institut Polytechnique de Paris, France.

---

## Abstract

In this work, we introduce a filtration on temporal graphs based on  $\delta$ -temporal motifs (recurrent subgraphs), yielding a multi-scale representation of temporal structure. Our temporal filtration allows tools developed for filtered static graphs, including persistent homology and recent graph filtration kernels, to be applied directly to temporal graph analysis. We demonstrate the effectiveness of this approach on temporal graph classification tasks.

## 2012 ACM Subject Classification

**Keywords and phrases** Temporal Graphs, Persistent Homology, Topological Data Analysis

## 1 Introduction

A nested sequence of spaces ( $X_1 \subseteq X_2 \subseteq \dots \subseteq X_n$ ) is referred to as a *filtration* and remains a simple yet highly effective idea for studying an object or space across multiple scales. It captures how features evolve from local to global structure. Persistent homology (PH) is a central example: by tracking homological features through a filtration, it yields a richer and more nuanced understanding of a space's topology. Recently, this idea of strengthening a discriminating invariant via filtration has been extended to graph learning through *graph filtration kernels* [23]. Schulz et al. [23] show that filtered graph kernels are strictly more expressive than static graph kernels, precisely because filtrations provide a unified yet fine-grained, and orderly representation of the underlying structure. This added expressiveness is especially relevant given that determining whether two graphs are isomorphic remains computationally challenging [3].

Given the significance and availability of general tools such as PH and filtered graph kernels—which rely on filtered representations—it is advantageous to analyze an object through a suitable filtration. In this article, we extend this perspective to the study of *temporal graphs* [13], where edges carry timestamps representing time-specific interactions. We propose a method that captures temporal connectivity without aggregating data into discrete snapshots, enabling each temporal graph to be treated as a single coherent entity. This provides a filtration-based alternative to snapshot-based methods [2, 9, 17, 25, 28], which often obscure the finer temporal structure.

**Our Approach:** We use  $\delta$ -temporal motifs, introduced in [19]—small connected temporal subgraphs whose edges occur within a  $\delta$ -time window (see Section 2 for the precise definition)—to define local distances between nodes. These distances induce a filtration that captures both the frequency and timing of interactions, formalized as the *average filtration* in Section 3. The use of  $\delta$ -temporal motifs is motivated by [19], which shows experimentally



© Samrik Chowdhury et al.;  
licensed under Creative Commons License CC-BY 4.0  
Leibniz International Proceedings in Informatics



LIPIC Schloss Dagstuhl – Leibniz-Zentrum für Informatik, Dagstuhl Publishing, Germany

that the distribution of various  $\delta$ -motifs differs significantly across classes of temporal graphs. More generally, local neighborhood structures are central to studying isomorphism properties of static graphs, as exemplified by the Weisfeiler–Lehman framework [26, 32].

We then use the resulting average filtration in two ways for temporal graph classification: first, by applying *persistent homology* to extract topological features such as connectivity and cycles, yielding a general-purpose descriptor (a *persistence diagram*, see Section 2); and second, by employing the recently introduced graph filtration kernels [23]. Both approaches produce kernel matrices that are subsequently used to train an SVM classifier.

**Our Contribution:** Our main contributions are as follows:

1. We introduce a filtration-based framework for representing and analyzing temporal graphs without relying on snapshot aggregation. Our method naturally handles temporal graphs of varying sizes and offers broader applicability than existing approaches that depend on node-level labels.
2. On the theoretical side, we establish the stability of our filtration under standard temporal graph reference models (see Section 4). We also provide an efficient algorithm for computing the average filtration with time complexity  $\mathcal{O}(|E| \times d_{\max})$  and memory usage comparable to that of an aggregated graph, offering substantial space savings relative to storing full temporal data. Here,  $|E|$  is the number of temporal edges and  $d_{\max}$  is the maximum temporal degree.
3. We extensively benchmark our framework for temporal graph classification, achieving over 92% accuracy in all settings and 100% in several cases (see Section 5), all without requiring node-level labels.

**Related work:** Temporal graphs have been widely used in applications ranging from ecological systems to human close-range interactions, collaboration networks, and biological signaling networks [4–6, 10, 13, 27]. Characterizing and classifying temporal graphs is an important and active research area, with approaches spanning kernel methods [18], embedding distances [8], temporal motifs [16, 19], and neural networks [21, 22].

Numerous metrics and tools exist for assessing structural properties of static graphs, and while some—such as path length, centrality, and betweenness—have been extended to temporal graphs [13], comparatively few methods analyze temporal graphs as holistic objects. Dall’Amico et al. [8] address this gap by defining a metric on the space of temporal graphs, allowing each temporal graph to be treated as a single entity. Our work extends this perspective by introducing a more general, filtration-based representation of temporal graphs, providing a more fine-grained framework for their comparison and analysis.

Ye et al. [33] also define filtrations for dynamic graphs and use the resulting persistence diagrams for classification. However, their model relies on time-varying edge weights to determine filtration values, yet—somewhat surprisingly—most of their experiments use unweighted graphs. This makes their approach appear less directly aligned with standard temporal networks, which are typically modeled as contact sequences. In the context of applying persistent homology to temporal data, Tinarrage et al. [28] and Myers et al. [17] employ zigzag PH to analyze temporal networks, with the former using discrete time-window resolutions for visualization. While effective, zigzag persistence is computationally expensive and highlights the difficulty of capturing temporal structure without aggregation, as well as the challenge of selecting meaningful temporal resolutions [28].

The work by Oettershagen et al. [18] introduces three distinct techniques for mapping temporal graphs to static graphs, thereby enabling the application of conventional static

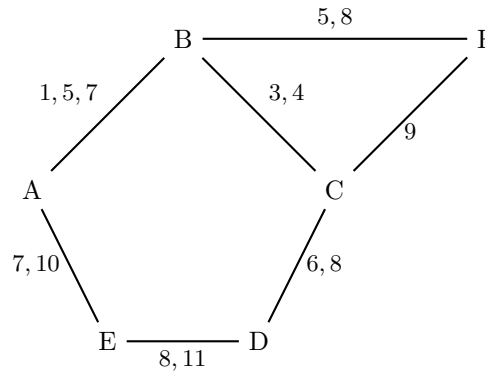
graph kernels. Wang [30] explore the classification of temporal graphs where both vertex and edge sets evolve over time. Tu et al. [29] leverage temporal motifs, while Wang et al. [31] propose time-variant graph classification via *graph-shapelet patterns* extracted from sequences of snapshot-based graph statistics.

## 2 Preliminaries

In this section, we briefly recall basic notions related to temporal networks, persistent homology and kernel methods. Readers may refer to [11–13, 24] for more details.

### 2.1 Temporal Network

**Temporal Graphs:** A **temporal graph** is defined as a tuple  $T = (V, E)$ , where  $V$  represents a set of vertices (nodes), and  $E$  is a set of directed or undirected *temporal edges*. Each temporal edge  $e := (u, v, t)$  connects vertices  $u$  and  $v$  and is active only at a specific time  $t$ . Alternatively, a temporal graph is as a sequence of contacts (interactions), where each temporal edge is represented as a contact  $(u, v, t)$ . If there is only a single temporal edge between any two nodes, the graph is referred to as a **single-labeled temporal graph**. When multiple temporal edges exist between two nodes, such as  $(u, v, t_1)$  and  $(u, v, t_2)$  etc., the graph is called a **multi-labeled temporal graph**. Collectively, these temporal edges are referred to as the edges between  $u$  and  $v$ . Furthermore, if all the edges (interactions) have a time duration  $[t_1, t_2]$ , the graph is known as an **interval temporal graph** and the temporal edge is denoted as  $e = (u, v, [t_1, t_2])$ . The **temporal degree** of a vertex  $u$  is the number of temporal edges connected to it, denoted by  $td_u$ . See Figure 1 for an example of multi-labeled temporal graph.

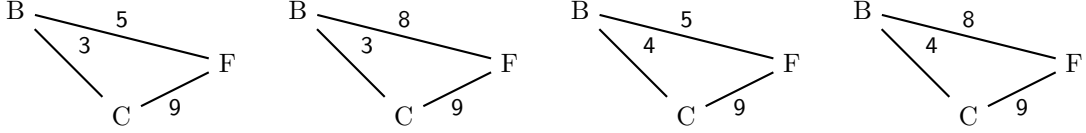


1 ■ **Figure 1** Multiple time labels are separated by commas.

For simplicity, this article focuses on undirected temporal graphs; however, all concepts and methods can naturally extend to directed temporal graphs. When the context is clear, a temporal edge is referred to simply as an *edge*. By ignoring timestamps and duplicate edges, a temporal graph induces a simple static graph, commonly referred to as the **aggregate graph**  $G$  of  $T$ . In  $G$ , a pair  $(u, v)$  is an edge if and only if there exists a temporal edge  $(u, v, t)$  in  $T$ .

**$\delta$ -Temporal Motifs:** We recall the definition of  $\delta$ -temporal motifs from [19] in the context of undirected temporal graphs. A  $k$ -node,  $l$ -edge,  $\delta$ -**temporal motif** is a sequence of  $l$  edges,

$M = \{(u_1, v_1, t_1), (u_2, v_2, t_2), \dots, (u_l, v_l, t_l)\}$  such that the edges are time-ordered within a  $\delta$  duration, i.e.,  $t_1 < t_2 < \dots < t_l$  and  $t_l - t_1 \leq \delta$ , and the induced aggregate graph from the edges is connected and has  $k$  nodes. Note that with this general definition, multiple edges between the same pair of nodes may appear in the motif  $M$ . However, we restrict our attention to the case where for any pair of temporal edges  $(u_i, v_i, t_i), (u_j, v_j, t_j)$  in  $M$ , it is not true that  $u_i = u_j$  and  $v_i = v_j$ <sup>1</sup>. See Figure 2 for examples.



3 **Figure 2** All four possible 3-node 3-edge motifs of Figure 1 are depicted here. Note that the  
 4 temporal edges between  $B$  and  $C$  and  $B$  and  $F$  differ in their respective timestamps. The two left  
 5 motifs satisfy  $\delta = 6$ , while the two right motifs satisfy  $\delta = 5$ .

## 2.2 Topological Data Analysis

**Simplicial Complex:** A  $k$ -**simplex** on a vertex set  $V$  is any subset  $\sigma \subseteq V$  with  $|\sigma| = k + 1$ , and every nonempty  $\tau \subseteq \sigma$  is called a **face** of  $\sigma$ . An **abstract simplicial complex**  $K$  is a collection of finite subsets of a vertex set such that  $\sigma \in K$  and  $\tau \subseteq \sigma \Rightarrow \tau \in K$ . Thus  $K$  is closed under taking faces. A **subcomplex** is any subcollection  $L \subseteq K$  that satisfies the same closure property. We will refer to an *abstract simplicial complex* as simply a *simplicial complex* or just a *complex*. A complex  $K$  is a **flag** or **clique** complex if, whenever a subset of its vertices forms a clique (i.e., any pair of vertices is connected by an edge), they span a simplex. It follows that the full structure of  $K$  is determined by its 1-skeleton (or graph), which we denote by  $G$ .

**Filtration:** A **sequence** of simplicial complexes  $\mathcal{F}: \{K_1 \hookrightarrow K_2 \hookrightarrow \dots \hookrightarrow K_m\}$  connected through inclusion maps is called a **filtration**. A filtration is called a **flag filtration** if all the simplicial complexes  $K_i$  are flag complexes. Given a weighted graph  $G = (V, E, w : E \rightarrow \mathbb{R})$ , a flag filtration  $F_G$  can be defined by assigning the maximum weight of edges in a simplex (clique) as its filtration value. Flag filtrations are among the most common types of filtrations used in TDA applications. As the filtration *parameter* increases, new simplices are added, allowing us to track topological features, such as Betti numbers, emerge and disappear across different scales. The next paragraph formalizes this intuition.

**Persistent Homology:** If we compute the homology groups of all the  $K_i$ , we obtain the sequence  $\mathcal{P}(\mathcal{F}): \{H_p(K_1) \xrightarrow{*} H_p(K_2) \xrightarrow{*} \dots \xrightarrow{*} H_p(K_m)\}$ . Here  $H_p()$  denotes the homology group of dimension  $p$  with coefficients from a field  $\mathbb{F}$ , and  $\xrightarrow{*}$  is the homomorphism induced by the inclusion map.  $\mathcal{P}(\mathcal{F})$  forms a sequence of vector spaces connected through the homomorphisms, called a **persistence module**.

Any persistence module can be *decomposed* into a collection of simpler interval modules of the form  $[i, j]$  [34]. The multiset of all intervals  $[i, j]$  in this decomposition is called the **persistence diagram** of the persistence module. An interval of the form  $[i, j]$  in the persistence diagram of  $\mathcal{P}(\mathcal{F})$  corresponds to a homological feature (a ‘cycle’) that appears at

2 <sup>1</sup> This restriction is necessary to define a filtration of simplicial complexes.

$i$  and disappears at  $j$ . The persistence diagram (PD) completely characterizes the persistence module, providing a bijective correspondence between the PD and the equivalence class (isomorphic) of the persistence module [11, 34].

### 2.3 PSS Kernel and Graph Filtration Kernel

**Kernel for Persistence Diagrams:** A kernel for persistence diagrams quantifies the similarity between diagrams by computing a weighted sum of inner products of feature points. A commonly used kernel for PDs is the Persistence Scale Space (PSS) Kernel. The **Persistence Scale Space (PSS) Kernel** [20] is defined for two persistence diagrams  $D$  and  $D'$  as follows:

$$K_{PSS}(D, D') = \frac{1}{8\pi\sigma^2} \sum_{(p \in D)} \sum_{(q \in D')} e^{(-\frac{1}{8\sigma}(\|p-q\|^2))} - e^{(-\frac{1}{8\sigma}(\|p-\bar{q}\|^2))},$$

where  $\sigma$  is a bandwidth parameter and  $\bar{q} = (b, a)$  is  $q = (a, b)$  mirrored at the diagonal. The PSS Kernel is stable under small perturbations of the input, ensuring that small changes in the diagram do not result in drastic kernel value changes, which is essential for robust applications in noisy data.

**Graph Filtration Kernel:** A **graph filtration** is a nested sequence of graphs  $G_1 \subseteq G_2 \subseteq \dots \subseteq G_k$ . For an edge-weighted graph  $G = (V, E, w)$  with  $w : E \rightarrow \mathbb{R}_{>0}$ , a standard filtration is obtained by thresholding the edge weights:  $A(G) : G_1 \subseteq G_2 \subseteq \dots \subseteq G_k = G$ , where each  $G_i = (V, E_i)$  is defined by  $E_i = \{e \in E : w(e) \geq \alpha_i\}$  for thresholds  $\alpha_1 \geq \alpha_2 \geq \dots \geq \alpha_k = 0$  (cf. [23]). Let  $F$  be a finite set of graph features (e.g., WL labels), and fix  $f \in F$ . The *filtration histogram*  $\phi_A^f(G) \in \mathbb{R}^k$  records the number of occurrences of  $f$  in each filtration level  $G_i$ :

$$\phi_A^f(G)_i = \#\{f \text{ in } G_i\}, \quad i = 1, \dots, k.$$

Let  $A_\alpha = \{\alpha_1, \dots, \alpha_k\}$  with ground distance  $d_1(\alpha_i, \alpha_j) = |\alpha_i - \alpha_j|$ , and let  $W_{d_1}$  denote the corresponding 1-Wasserstein distance. Using the  $\ell_1$ -normalized histogram  $\hat{\phi}_A^f(G) = \phi_A^f(G) / \|\phi_A^f(G)\|_1$ , the *base filtration kernel* for feature  $f$  and  $\gamma > 0$  is

$$k_f^A(G, G') = \exp\left(-\gamma W_{d_1}\left(\hat{\phi}_A^f(G), \hat{\phi}_A^f(G')\right)\right). \quad (1)$$

The *graph filtration kernel* aggregates these base kernels using the original histogram masses:

$$K_{F,A}^{\text{Filt}}(G, G') = \sum_{f \in F} k_f^A(G, G') \|\phi_A^f(G)\|_1 \|\phi_A^f(G')\|_1. \quad (2)$$

Intuitively, this kernel measures similarity by comparing how features appear and evolve across the filtration. The filtration kernel is strictly more expressive than its base feature map (e.g., WL subtree features) because it captures how features evolve along the filtration. As shown in [23], graphs that standard histogram-based kernels cannot distinguish become separable when their filtration histograms are compared via the Wasserstein distance.

## 3 Temporal Filtrations

In this section, we introduce a simple method and an algorithm for constructing filtered (weighted) graphs from single-labeled, and multi-labeled temporal graphs. The filtered graph captures the evolution of fixed-size (3-node, 2-edge)  $\delta$ -temporal motifs.

### 3.1 Single Labeled Temporal Graphs

**The Average Filtration:** Let  $T = (V, E)$  be a single-labeled temporal graph, we construct a filtered simple graph  $G_f = (V_f, E_f, f_{\text{avg}} : (V_f \cup E_f) \rightarrow \mathbb{R})$  derived from  $T$ . The vertex set  $V_f$  of  $G_f$  is identical to  $V$ , and the edge set  $E_f$  of  $G_f$  corresponds to the edges in the aggregate graph  $G$  of  $T$ . Specifically, for each temporal edge  $(u, v, t) \in E$  in  $T$ , there exists a corresponding edge  $(u, v) \in E_f$  in  $G_f$ . Notably,  $G_f$  is a simple graph, meaning that no multiple edges exist between any pair of vertices. The filtration  $f_{\text{avg}} : (V_f \cup E_f) \rightarrow \mathbb{R}$  is referred to as the **average filtration**.

To motivate the definition of the average filtration  $f_{\text{avg}}$ , we first introduce the concept of the **minimum filtration**  $f_{\text{min}} : (V_f \cup E_f) \rightarrow \mathbb{R}$ . We begin by assigning a filtration value of 0 to all vertices in  $V_f$ , i.e.,  $f_{\text{avg}}(V_f) = 0$ . We then describe the method for computing the filtration values of the edges in  $G_f$ .

Let  $\mathcal{N}_T(u, v) := \{(u', v', t) \mid u = u' \text{ or } v = v'\} \setminus \{(u, v, t)\}$  represent the set of adjacent temporal edges of  $(u, v, t)$  in  $T$ , where each interaction  $(u, v, t)$  belongs to  $T$ . Additionally, let  $\tau(u, v) := t$  denote the time label of the edge  $(u, v)$  in  $T$ . The filtration value of each edge  $(u, v)$  in  $G_f$  is computed using the minimum of the difference in time stamps between the edge  $(u, v)$  and its adjacent interactions in  $T$ :

$$f_{\text{min}}(e) := \min_{e' \in \mathcal{N}_T(e)} |\tau(e) - \tau(e')|.$$

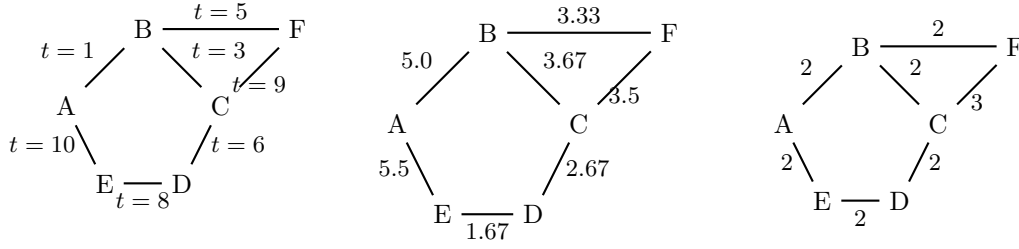
As previously mentioned, we aim to capture the evolution of  $\delta$ -temporal motifs within a temporal graph through temporal filtrations. By fixing the values of  $k$  (number of nodes) and  $l$  (number of edges), one can canonically define a filtration over the temporal graph by varying the parameter  $\delta$ . Specifically, for each edge  $(u, v)$  in a temporal graph, its filtration value is assigned as the smallest  $\delta$  for which it belongs to a fixed  $k$  and  $l$   $\delta$ -temporal motif. For  $k = 3$  and  $l = 2$ , this canonical filtration corresponds to the minimum filtration  $f_{\text{min}}$ , as defined above. The minimum filtration  $f_{\text{min}}$  is highly sensitive to changes in interactions, particularly those corresponding to the minimum value, and it often fails to robustly capture the relational and global ‘temporal connectivity’ of the graph. To address this limitation, we redefine the filtration value of an edge as the average of all  $\delta$ -values in the smallest (w.r.t to the parameter  $\delta$ )  $\delta$ -temporal motifs that include the edge. Specifically, the *average filtration* of the edges in  $G_f$  is defined as:

$$f_{\text{avg}}(e) := \frac{\sum_{e' \in \mathcal{N}_T(e)} |\tau(e) - \tau(e')|}{|\mathcal{N}_T(e)|}.$$

The average filtration reflects the relative temporal importance of an edge: a smaller filtration value indicates that more and faster temporal paths pass through the edge.

The examples in Figure 3 illustrate the distinction between the average and minimum filtrations. The temporal loop  $ABCDEA$  in the original temporal graph (left of Figure 3) has a temporal length of 9 and can be constructed from smaller  $\delta$ -temporal motifs with 3 nodes and 2 edges for  $\delta = 9$ . However, in the minimum filtration, the cycle appears at  $\delta = 2$ , while in the average filtration, it emerges at  $\delta = 5.5$ . Additionally, the average filtration produces more widely distributed filtration values. This difference suggests that the average filtration takes into account a broader neighborhood around each edge, assigning values that more accurately reflect the relative ‘temporal position’ of the edges. This characteristic makes the average filtration more stable and discriminative compared to the minimum filtration. Experimental results further validate this observation.

We fix the size of the  $\delta$ -temporal motifs to be 3-node, 2-edge, as it is the smallest (and perhaps only) motif that captures the complete global connectivity of the temporal graph.



6 **Figure 3** The first figure on the left shows a single-labeled temporal graph, followed by the  
 7 corresponding average and minimum filtrations derived from it in the next two figures.

The example in Figure 2 clearly illustrates this; all possible 3-node, 3-edge  $\delta$ -temporal motifs in the figure would fail to cover the entire temporal graph.

**Algorithm:** We present an efficient algorithm for computing the average filtration of a temporal graph  $T = (V, E)$ . The main idea of the algorithm is as follows: we first iterate over the vertices  $V$  of the graph. For each vertex  $v \in V$ , we examine the set of edges  $E_v \subset E$  incident to  $v$ . Any two such incident edges  $e$  and  $e'$  will be adjacent and will contribute to each other's filtration values. Specifically, for each pair of incident edges, we compute the timestamp difference  $|t - t'|$ , where  $t$  and  $t'$  are the respective timestamps of  $e$  and  $e'$ .

To efficiently track these contributions, we maintain a sum variable  $S_e$  for each edge  $e$ . After calculating  $|t - t'|$ , we update the sum variables for both edges as follows:  $S_e \leftarrow S_e + |t - t'|$  and  $S_{e'} \leftarrow S_{e'} + |t - t'|$ . This process is repeated for all possible pairs of incident edges on  $v$ , and the vertex  $v$  is then marked as visited. Once both boundary vertices of an edge  $e = uv$  are marked as visited, we compute its filtration value:  $f_{\text{avg}}(e) = \frac{S_e}{td_u + td_v}$ , where  $td_u$  and  $td_v$  are the temporal degrees of the vertices  $u$  and  $v$ , respectively. See the pseudocode (Algorithm 1) for more details.

To optimize the computation of incident temporal edges at each vertex, the graph is stored as an adjacency linked list of edges incident to each vertex  $v$ . This representation allows the retrieval of  $E_v$  in constant  $\mathcal{O}(1)$  time. For each vertex, we compare  $\mathcal{O}(d_{\text{max}}^2)$  pairs of incident edges, where  $d_{\text{max}}$  is the maximum temporal degree of the graph. Consequently, the overall time complexity of the algorithm is:  $\mathcal{O}(|V| \times d_{\text{max}}^2) = \mathcal{O}(|E| \times d_{\text{max}})$ , where  $|V|$  is the total number of vertices and  $|E|$  is the total number of temporal edges in the graph.

### 3.2 Multi-labeled Temporal Graphs

We now extend the average filtration of single-labeled temporal graphs to multi-labeled temporal graphs. Our approach for multi-labeled graphs follows a similar methodology as the single-labeled case. In this context, we average the time differences across multiple interactions and assign a single edge to represent the interactions.

Given a multi-labeled temporal graph  $T = (V, E)$ , we construct a filtered simple graph  $G_f = (V_f, E_f, f_{\text{avg}}^{\text{mlt}} : (V_f \cup E_f) \rightarrow \mathbb{R})$  derived from  $T$ . Similar to the single-labeled case, the vertex set  $V_f$  and the edge set  $E_f$  of  $G_f$  correspond to the vertices and edges in the aggregate graph  $G$  of  $T$ . Here,  $\tau(u, v) = \{t \mid (u, v, t) \in E\}$  represents the set of all time labels associated with the edge  $(u, v)$ . As in the single-labeled case, the filtration value of vertices is set to 0. The filtration value of the edges in  $G_f$  is computed as follows:

$$f_{\text{avg}}^{\text{mlt}}(e) = \frac{\sum_{e' \in \mathcal{N}_T(e)} \sum_{t \in \tau(e), t' \in \tau(e')} |t - t'|}{|\mathcal{N}_T(e)|}.$$

---

8 **Algorithm 1** ComputeAverageFiltration

---

```

9 1: Initialize  $S_e \leftarrow 0$  for each  $e \in E$  and  $\text{visited}_v \leftarrow \text{False}$  for each  $v \in V$ 
10 2: Initialize an empty filtration value map  $f_{\text{avg}}$ 
11 3: for each vertex  $v \in V$  do
12 4:   Retrieve all incident edges  $E_v = \{e = (v, u, t)\}$ 
13 5:   Initialize a stack stack with all edges  $e \in E_v$ 
14 6:   while stack is not empty do
15 7:     Pop an edge  $e = (v, u, t)$  from stack
16 8:     for each remaining edge  $e' = (v, w, t')$  in stack do
17 9:       Compute  $\Delta \leftarrow |t - t'|$ 
18 10:      Update  $S_e \leftarrow S_e + \Delta$ 
19 11:      Update  $S_{e'} \leftarrow S_{e'} + \Delta$ 
20 12:    end for
21 13:    if  $\text{visited}_u = \text{True}$  then ▷  $v$  being visited is not required
22 14:      Compute  $f_{\text{avg}}(e) \leftarrow \frac{S_e}{td_v + td_u}$ 
23 15:    end if
24 16:  end while
25 17:  Mark  $\text{visited}_v \leftarrow \text{True}$ 
26 18: end for
27 19: return  $f_{\text{avg}}(e)$  for all  $e \in E$ 

```

---

## 4 Stability

In this section, we examine the stability of the temporal filtrations defined earlier in the context of *randomized reference models* of temporal graphs. To provide a foundation, we first briefly review the concept of randomized reference models and introduce some commonly used models, as outlined in [13, 14]. These models form the basis for defining the various classification classes used in our experiments.

### 4.1 Randomized Reference Model

The *configuration model* is a randomized reference model, commonly used in the study of static networks to compare the empirical network's features (such as clustering, path length, or other topological characteristics) with those of a randomized network. The configuration model is created by randomly shuffling the edges of a given graph while preserving some of its structural properties, most notably the degree distribution.

For temporal graphs, a similar approach involves randomizing or reshuffling event sequences (interactions) to remove time-domain structures and correlations. Unlike static networks, temporal graphs exhibit diverse temporal correlations (structures) across varying scales, making it challenging to design a single, universal null model. Karsai et.al. [14] identify five of these temporal correlations, namely: community structure (C), weight-topology correlations (W), bursty event dynamics on single links (B), and event-event correlations between links (E) and a daily pattern (D). They also provide tailored null models that selectively remove specific correlations to analyze their influence on the observed temporal features or dynamical processes like spreading. Below, we recall three temporal null models from Karsai et al. [14] and Holme [13].

- **Equal-Weight Link-Sequence Shuffle (EWLSS):** In this method, two interaction

pairs  $(u_1, v_1), (u_2, v_2) \in V \times V$  are randomly selected such that  $|\tau(u_1, v_1)| = |\tau(u_2, v_2)|$ . Then the time labels of these selected pairs  $(u_1, v_1)$  and  $(u_2, v_2)$  are swapped. Note that,  $\tau(u, v)$  represents the set of time labels associated with the pair  $(u, v)$ . This process can be repeated multiple times to construct a new randomized temporal graph.

- **Randomized Edges (RE):** Algorithmically this method could be described as follows: iterate over all edges and for each edge  $(u, v)$ , select another edge  $(u', v')$ . With 50% probability, replace  $(u, v)$  and  $(u', v')$  with  $(u, v')$  and  $(u', v)$ ; otherwise, replace them with  $(u, u')$  and  $(v, v')$ . The times of contact for each edge remain constant and we further make sure that there are no self loops or multiple edges.
- **Configuration Model (CM):** The aggregated graph of the temporal graph is rewired using the configuration model of the static graph, which preserves the degree distribution and overall connectivity of nodes while removing topological correlations. Then the original single-edge interaction time labels are randomly assigned to the edge, followed by time shuffling. This method destroys all correlations except broad seasonal patterns, such as daily cycles.

In addition to these three model we introduce a new null model that is suitable for some of our specific experiments.

- **Time Perturbation (TP):** In this method, a fraction of interactions  $e = (u, v, t) \in E$  in the original temporal graph is replaced with  $e' = (u, v, t')$ , where  $|t - t'| < \epsilon$  for some  $\epsilon > 0$ . This procedure only perturbs the time stamps of the edges, preserving most of the temporal and structural features of the original temporal graph.

The first model, EWLSS, preserves the daily pattern (D), the community structure (C), weight-topology correlations (W), and bursty event dynamics on individual edges (B). In contrast, the configuration model loses all temporal correlations (structures) except for the daily pattern (D). This distinction has been experimentally verified by Karsai et al. [14], where graphs generated using EWLSS procedures exhibit spreading dynamics closely resembling those of the original graph. On the other hand, graphs generated using the configuration model deviate significantly from the original dynamics.

We leverage these models to define and populate distinct classes for classification tasks. The configuration model generates temporal graphs with diverse dynamics, while the other three models (EWLSS, RE and TP) are used to produce graphs with similar dynamics, forming a single class. The similarity within each class depends on the model used; TP and EWLSS create more homogeneous classes compared to the RE model. Originally designed for studying spreading dynamics with the SI model [15], these null models eliminate the need for direct SI simulations, enhancing both the efficiency and flexibility of our method without requiring labeled nodes.

## 4.2 Stability

We now discuss the stability of our temporal filtration with respect to the above null models. In particular, we calculate the difference in the average filtrations values of the edges that are , shuffled, swapped or changed during each step of the above reference modes.

**TP Procedure :** Let  $T$  be a single-labeled temporal graph and  $e = (u, v, t)$  is an interaction in  $T$ . Suppose the time label  $\tau(e) = t$  is replaced by  $t + \epsilon$ . The change in  $f_{\text{avg}}(e)$ , denoted by  $\Delta f_{\text{avg}}(e)$ , can be upper bounded as follows:

## XX:10 Filtration-Based Representation Learning for Temporal Graphs

$$\begin{aligned}\Delta f_{\text{avg}}(e) &= f_{\text{avg}}(e)_{\text{new}} - f_{\text{avg}}(e)_{\text{old}} \\ &= \frac{1}{|\mathcal{N}_T(e)|} \sum_{e' \in \mathcal{N}_T(e)} \left( |(t + \epsilon) - \tau(e')| - |t - \tau(e')| \right).\end{aligned}$$

Let  $\tau(e') = t'$ , then for each  $e' \in \mathcal{N}_T(e)$  the inner term is  $|(t + \epsilon) - t'| - |t - t'| \leq \epsilon$ . we therefore obtain:  $|\Delta f_{\text{avg}}(e)| \leq \epsilon$ . The filtration values of edges in the neighborhood of  $e$  also change. Using a similar computation and the fact that  $\tau(e'')$  does not change for all  $e'' \in \mathcal{N}_T(e') \setminus \{e\}$ , for each  $e' \in \mathcal{N}_T(e)$ , we can express the change as:

$$\Delta f_{\text{avg}}(e') = \frac{1}{|\mathcal{N}_T(e')|} (|(t + \epsilon) - \tau(e')| - |t - \tau(e')|) = \frac{\epsilon}{|\mathcal{N}_T(e')|} \leq \epsilon.$$

We use the  $L_\infty$  norm to measure the distance between filtrations [7]. The overall distance between the new (shifted) and the original average filtration of the temporal graph  $G$  is bounded above as follows:  $|\Delta_\infty f_{\text{avg}}(G)| \leq \epsilon$ . Note that this bound holds even after time stamp shifts of multiple edges.

For simplicity, we have assumed that  $T$  is a single-labeled temporal graph. However, through a similar calculation, it can be shown that the same bound applies to multi-labeled temporal graphs and cases where multiple time labels of an edge are shifted. Since the underlying aggregate graph remains unchanged after a TP procedure, the stability theorem [7] guarantees stability in the resulting persistence diagrams.

**EWLSS Procedure:** To upper bound the differences in the average filtration when swapping time labels  $t_1$  and  $t_2$  for the edges  $e_1 = (u_1, v_1, t_1)$  and  $e_2 = (u_2, v_2, t_2)$ , we proceed as follows:

$$\text{For } e_1 : \Delta f_{\text{avg}}(e_1) = \frac{\sum_{e' \in \mathcal{N}_T(e_1)} (|t_2 - \tau(e')| - |t_1 - \tau(e')|)}{|\mathcal{N}_T(e_1)|}.$$

Again we can bound the inner term,  $\left| |t_2 - \tau(e')| - |t_1 - \tau(e')| \right| \leq |t_2 - t_1|$ , Thus:

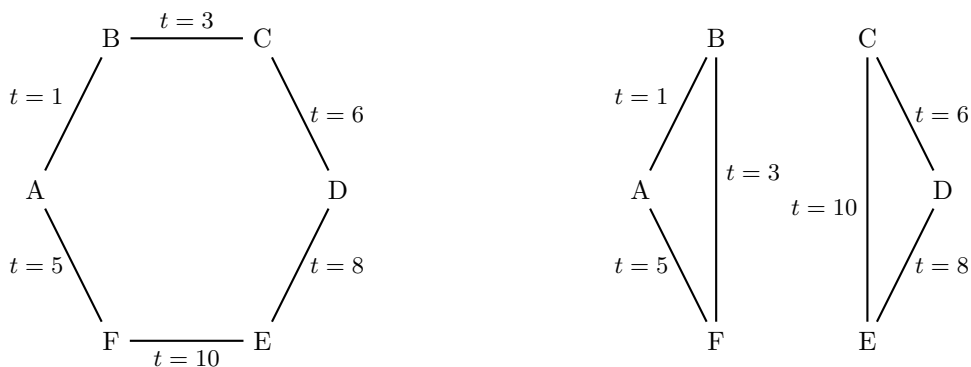
$$|\Delta f_{\text{avg}}(e_1)| \leq \frac{|\mathcal{N}_T(e_1)| \cdot |t_2 - t_1|}{|\mathcal{N}_T(e_1)|} = |t_2 - t_1|.$$

By symmetry,  $|\Delta f_{\text{avg}}(e_2)| \leq |t_2 - t_1|$ . The filtration values of the edges in the neighborhoods  $\mathcal{N}_T(e_1)$  and  $\mathcal{N}_T(e_2)$  of  $e_1$  and  $e_2$ , respectively, will also change. However, these changes will be bounded above by  $|t_2 - t_1|$ .

For a single pair swap, the absolute distance between the average filtration of the swapped graph and the original graph is bounded as:  $|\Delta_\infty f_{\text{avg}}(G)| \leq |t_2 - t_1|$ . For multiple pair swaps, the distance is bounded above by the maximum time label difference among the pairs:  $|\Delta_\infty f_{\text{avg}}(G)| \leq \max |t_2 - t_1|$ . As in the previous case, the underlying aggregate graph remains unchanged after an EWLSS procedure. Consequently, the persistence diagrams remain stable as well.

**RE and CM Procedure:** The average filtration does not exhibit theoretical stability for the remaining two procedures, RE and configuration models. This behavior is expected, primarily because the underlying aggregate graphs could change at each step of these procedures. Such

changes result in an infinite difference between the filtration values of previously non-existent interactions and those of newly added interactions or vice-versa. We illustrate this change for the RE procedure in Figure 4. Among the RE and configuration models, RE generates more similar temporal graphs. Therefore, to design a relatively heterogeneous class, we still use the RE procedure to populate a single class.



28 **Figure 4** An example of a single step in the RE procedure involves shuffling the edges  $BC$  and  
 29  $FE$  to  $BF$  and  $CE$ , respectively, while maintaining their original time stamps.

## 5 Experiments

In this section, we present experiments to evaluate the effectiveness of our method in classifying temporal graphs.

**Pipelines:** Our benchmarking of temporal graph classification uses two pipelines:

- a) **Persistent Homology pipeline:** For each temporal graph, we compute the average filtration and its corresponding flag filtration, from which we extract persistence diagrams up to degree 2. For each degree, we compute a kernel distance matrix using the Persistence Scale Space kernel [20], yielding three matrices (degrees 0–2). These are combined with equal weights<sup>2</sup> to form a single kernel matrix, which is then used to train an SVM classifier.
- b) **Graph filtration kernel pipeline:** For each temporal graph, we compute the average filtration along with the static graph filtrations of [23] for benchmarking. We then apply the filtered Weisfeiler–Lehman kernel [23] to obtain a kernel matrix, which is used to train an SVM classifier. Except for computing the average filtration, all subsequent steps use the implementation provided in the source code of [23].

**Class Population:** To train the SVM classifier, we require at least two classes of temporal graphs. We follow a method similar to [8] to generate and populate these classes. Real datasets typically provide only a single temporal graph (the **root graph**), whereas synthetic datasets may contain one or more root graphs. The TP, EWLSS, and RE procedures (Section 4) generate loosely similar copies of a root graph, while the CM procedure produces distinct ones. This distinction is experimentally verified in [14] through SI-model simulations and analysis of infected-node distributions. For real datasets with a single root graph, two

30 <sup>2</sup> Different weights allow adjusting the influence of each degree.

## XX:12 Filtration-Based Representation Learning for Temporal Graphs

classes are formed: one of loose copies and one of CM-generated graphs<sup>3</sup>. With multiple root graphs, each root graph yields its own class through its loose copies.

**Datasets:** We summarize below the four real contact-sequence datasets used to benchmark our method. All datasets are sourced from the SocioPatterns repository [1].

Dataset	$ V $	$ E_s $	$ E $	$E_{avg}$	$E_{max}$	$d_{avg}$	$d_{max}$
Highschool 2011	126	1710	28540	16.69	1185	27.14	55
Highschool 2012	180	2220	45047	20.29	1280	24.67	56
Hospital Combined	75	1139	32424	28.47	1059	30.37	61
Workplace v2	217	4274	78249	18.31	1302	39.39	84

**Table 1**  $|V|$  denotes the number of vertices,  $|E_s|$  the number of edges in the aggregate graph, and  $|E|$  the number of temporal edges.  $E_{avg}$  and  $E_{max}$  are the average and maximum number of time labels per edge, while  $d_{avg}$  and  $d_{max}$  are the average and maximum temporal degrees of the nodes.

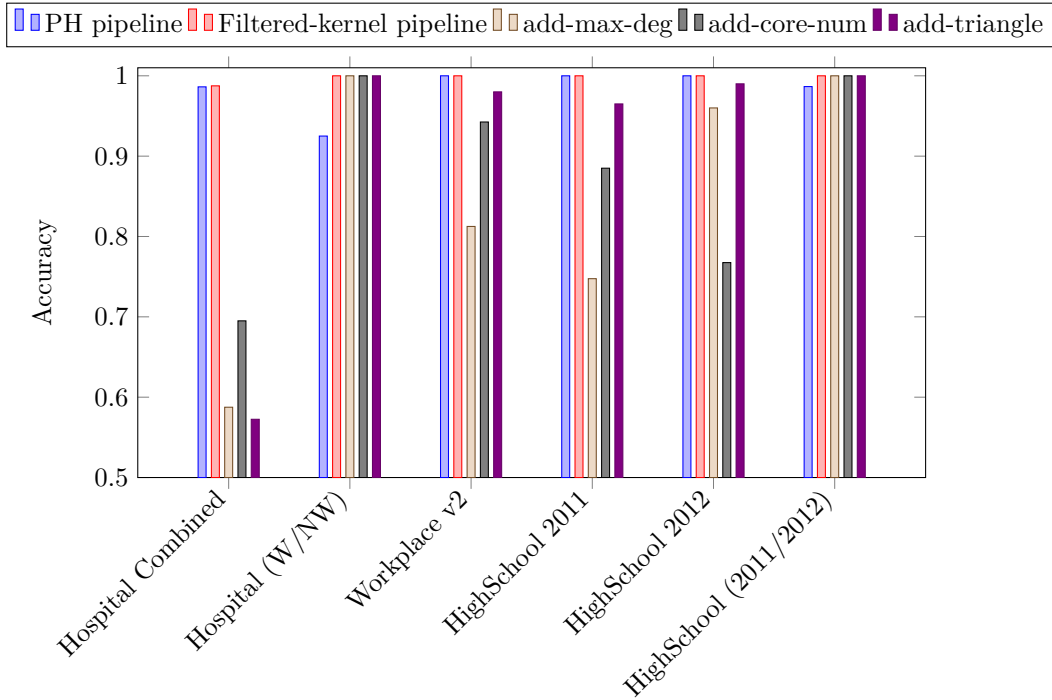


**Figure 5** Comparison of the PH and filtered-kernel pipelines across datasets. The reported accuracy scores are averaged over multiple runs, with only marginal variation across trials.

**Benchmark Accuracies:** The histogram in Figure 5 shows the classification accuracies from our experiments. The two temporal-graph classes were generated as described in the

<sup>3</sup> There are (at least) two possible ways to generate multiple classes. In the first, a CM-generated variant of the root graph serves as the representative of the second class, and both classes are populated using RE, TP, or EWLSS. In the second, the root graph represents the first class and is populated by loose copies, while the second class is formed by multiple distinct CM-generated variants. Thus, the first class contains similar graphs, whereas the second contains structurally different ones.

*Class population* paragraph above. Each dataset was split into training and testing sets using an 80–20 ratio, and accuracy was computed on the testing set as the proportion of correctly classified instances. The source code for all experiments using PH-pipeline is publicly available on GitHub at the following link.

Both the PH pipeline and the filtered-kernel pipeline use the average filtration<sup>4</sup> for classification. In addition, the filtered-kernel pipeline incorporates three static-graph filtrations from [23]: `add-max-deg`, `add-core-num`, and `add-triangle`<sup>5</sup>. The average filtration consistently provides strong classification performance, while the static filtrations also perform well when the aggregate graph structures of the classes differ sufficiently. For example, the Hospital (W/NW) dataset consists of two classes obtained from distinct segments of the Hospital Combined data—the working (staff) and non-working (patient) segments—and their structural differences lead to high accuracy for the static kernels. A similar trend is observed in the HighSchool (2011/2012) experiments.

**Similar Classes.** We also benchmarked the PH and filtered-kernel pipelines using the average filtration in settings where the two classes are highly similar—that is, the second-class representative is generated as a loose copy of the root graph using additional RE or EWLS steps<sup>6</sup>. In such cases, the temporal graphs are extremely similar, making the classes inherently difficult to distinguish. This is reflected in our experimental results (Table 2), further supporting the use of reference models to induce meaningful class differences.

	Dataset	Classes	PH		Filtered Kernel	
			Acc.	Std.	Acc.	Std.
54						
55						
56	Hospital Combined	RE + RE	0.5075	0.0842	0.5625	0.0709
57	Hospital Combined	EWLS + EWLS	0.5325	0.0693	0.5275	0.0425
58	HighSchool 2011	RE + RE	0.4588	0.0534	0.4450	0.0620
59	HighSchool 2011	EWLS + EWLS	0.5050	0.0707	0.4850	0.0784
60	HighSchool 2012	RE + RE	0.5063	0.0574	0.5375	0.0491
61	HighSchool 2012	EWLS + EWLS	0.4963	0.0502	0.4800	0.0620

62 ■ **Table 2** In the second column, “RE+RE” indicates that both classes are generated using the RE  
63 procedure on the root graph; other entries follow the same convention.

**Synthetic Datasets:** Next, we evaluate the PH pipeline on synthetic contact-sequence datasets (see Table 3). We use three root graphs with varying parameters, generated under both *disassortative* and *assortative* mixing strategies [13], modeling contact and disease-transmission dynamics.

46 <sup>4</sup> All temporal graphs in our experiments (except the random temporal graph experiment) are multi-labeled,  
47 and we use the  $f_{\text{avg}}^{\text{mlt}}$  filtration for both pipelines, as described in Section 3.

48 <sup>5</sup> The `add-max-deg` filtration assigns to each edge the maximum degree of its two endpoints in the  
49 aggregate graph. The `add-core-num` filtration uses the core numbers of the endpoints, where the core  
50 number of a node is the largest  $k$  such that it belongs to a  $k$ -core (subgraph in which all nodes have  
51 degree at least  $k$ ); an edge is assigned the maximum core number of its endpoints. The `add-triangle`  
52 filtration assigns to each edge half of the maximum number of triangles incident to either endpoint.

53 <sup>6</sup> Extra RE/EWLS steps were used to generate the second-class representative.

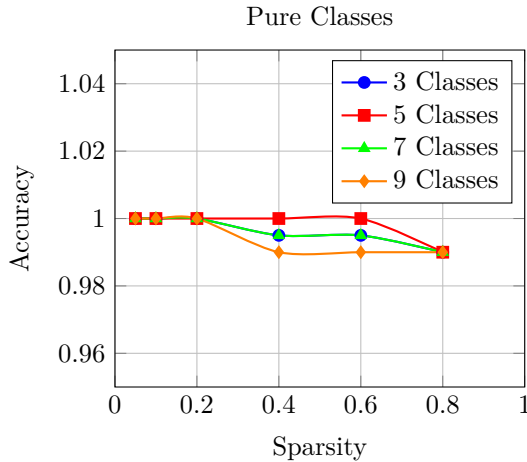
## XX:14 Filtration-Based Representation Learning for Temporal Graphs

Class	$ V / E $	Threshold	Average Accuracy	Average Stdev
3	100/200	0	0.9733	0.0235
3	250/500	0	1.0000	0.0000
3	100/1000	0	0.9681	0.0283

64  
65  
66  
67  
68 **Table 3** Results are averaged over 5 runs. On average, generating a new class member requires  
69 20 RE steps in the first two experiments and 32.5 steps in the last one.

**Random Temporal Graphs:** Figures 6 and 7 present the results of experiments on random temporal graphs using single-labeled graphs and the PH pipeline. These graphs do not model any specific phenomena. These experiments assess our method’s performance with many similar or mixed classes, as well as under varying temporal sparsity. For class generation, we use the TP procedure from Section 4: *out shifts* apply TP to a fraction of interactions to create distinct classes, while *in shifts* apply TP to a smaller fraction of edges within a single class. Details for each experiment are given in the figure descriptions.

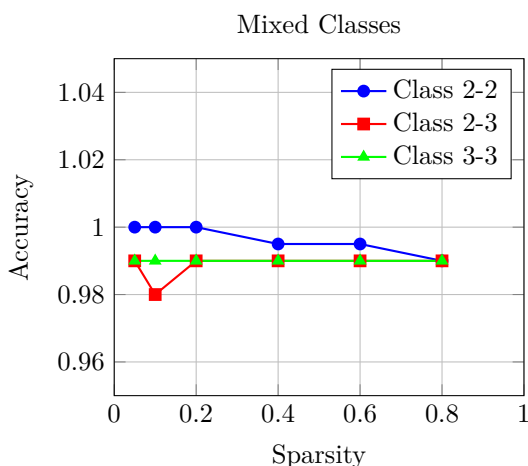
- a) **Pure Classes:** To create a homogeneous pool of classes, we generated a single-labeled temporal graph  $G$  with 100 vertices and varying sparsity (0.05 to 0.8), with time stamps in the range  $(0, 100]$ . For each experiment, the original root graph was used to create 3, 5, 7, or 9 new root graphs (classes) by shifting the time stamps (out-shifts) of an average of 4.75% of interactions by  $1 \leq \epsilon \leq 5$ . To populate graphs within the same class, time stamps of an average of 1.6% of interactions were shifted (in-shifts) by  $1 \leq \epsilon \leq 5$ .



For each class and sparsity pair, we ran four experiments with different out- and in-shift combinations, and the results for each combination were averaged over 5 runs. As the sparsity increases, the accuracy remains stable around 1.0 for all classes, with only minor drops at higher sparsity values. This indicates that the classification models maintain high performance even with lower data density.

70 **Figure 6** Accuracy vs. sparsity for different number of pure classes.

- b) **Mixed Classes:** For mixed class sets, we used two single-labeled temporal graphs  $G$ , each with 100 vertices, sparsity between 0.05 and 0.8, and time labels in  $(0, 100]$ . This setup yields both similar and distinct classes. For instance, Class 2–2 includes two classes from a root graph and its out-shifted variant, and similarly two from a second root graph. Classes 2–3 and 3–3 were generated in the same way. Out-shifts changed on average 4.75% of interactions ( $1 \leq \epsilon \leq 5$ ), while in-shifts affected about 1.88% within the same range.



For each class and sparsity pair, we conducted four experiments with different out- and in-shift combinations, averaging the results over five runs. The observed trends were consistent with the previous experiment (Figure 6), indicating that our classification model performs effectively in the mixed setup as well.

71 ■ **Figure 7** Accuracy vs. sparsity for different number of mixed classes.

**Implementation Details:** All experiments were implemented in Python, with C++ used to compute the kernel matrices and the  $f_{\text{avg}}^{\text{mlt}}$  filtration for multi-labeled temporal graphs. Experiments were run on a server equipped with an Intel(R) Core(TM) i7-6950X CPU and dual NVIDIA GeForce RTX 2080 Ti GPUs to ensure consistent runtime and accuracy comparisons.

**Future Work:** The idea of defining a filtration on a temporal graph naturally extends to higher-order motifs, interval-based temporal graphs, and probabilistic interactions, opening several avenues for future work on dynamic systems. With the recent addition of filtered graph kernels to the toolkit, our methodology further supports the development of Topological Machine Learning (TML) for temporal data, with potential applications in epidemic modeling, social networks, and financial systems.

## Acknowledgement

We thank Priyavrat Deshpande, Writika Sarkar, Mohit Upmanyu, and Shubhankar Varshney for their valuable input during the early discussions of the project.

## Funding

Last three authors received partial support from a grant provided by Fujitsu Limited. Part of this work was carried out during the second author’s visit to The University of Newcastle, NSW, Australia, and was partially funded by an ARC Discovery Grant (Grant Number: G2000134).

## References

- 1 Sociopatterns datasets, 2024. Accessed: 2024-12-02. URL: <http://www.sociopatterns.org/datasets/>.
- 2 M. Araujo, S. Papadimitriou, S. Günnemann, C. Faloutsos, P. Basu, A. Swami, E. E. Papalexakis, and D. Koutra. Com2: Fast automatic discovery of temporal ('comet') communities. In *Proceedings of the Pacific-Asia Conference on Knowledge Discovery and Data Mining (PAKDD)*, 2014.
- 3 László Babai. Graph isomorphism in quasipolynomial time. In *Proceedings of the 48th Annual ACM Symposium on Theory of Computing (STOC)*, pages 684–697, 2016. doi:10.1145/2897518.2897542.
- 4 Alain Barrat, Ciro Cattuto, Jameson L. Toole, and Lorenzo Isella. Empirical temporal networks of face-to-face human interactions. *European Physical Journal Special Topics*, 222(6):1295–1309, 2013. doi:10.1140/epjst/e2013-01910-9.
- 5 Benjamin Blonder, Tina W. Wey, Anna Dornhaus, Richard James, and Andrew Sih. Temporal dynamics and network analysis. *Methods in Ecology and Evolution*.
- 6 Ciro Cattuto, Wouter Van den Broeck, Alain Barrat, Vittoria Colizza, Jean-François Pinton, and Alessandro Vespignani. Dynamics of person-to-person interactions from distributed rfid sensor networks. *PLoS ONE*, 2010.
- 7 David Cohen-Steiner, Herbert Edelsbrunner, and John Harer. Stability of persistence diagrams. *Discrete & Computational Geometry*, 37(1):103–120, 2007.
- 8 Lorenzo Dall'Amico, Alain Barrat, and Ciro Cattuto. An embedding-based distance for temporal graphs. *Nature Communications*, 15(1):9954, 2024.
- 9 D. M. Dunlavy, T. G. Kolda, and E. Acar. Temporal link prediction using matrix and tensor factorizations. *ACM Transactions on Knowledge Discovery from Data (TKDD)*, 2011.
- 10 Nathan Eagle, Alex Pentland, and David Lazer. Inferring friendship network structure by using mobile phone data. *Proceedings of the National Academy of Sciences*, 2009.
- 11 Herbert Edelsbrunner and John Harer. *Computational Topology: An Introduction*. American Mathematical Society, Providence, RI, 2010.
- 12 Allen Hatcher. *Algebraic Topology*. Cambridge University Press, Cambridge, UK, 2002. URL: <https://pi.math.cornell.edu/~hatcher/AT/ATpage.html>.
- 13 Petter Holme and Jari Saramäki. Temporal networks. volume 519, pages 97–125, 2012. doi:10.1016/j.physrep.2012.03.001.
- 14 M. Karsai, M. Kivela, R. K. Pan, K. Kaski, J. Kertész, A.-L. Barabási, and J. Saramäki. Small but slow world: How network topology and burstiness slow down spreading. *Physical Review E*, 83, 2011.
- 15 William Ogilvy Kermack and Anderson G. McKendrick. A contribution to the mathematical theory of epidemics. *Proceedings of the Royal Society of London. Series A, Containing Papers of a Mathematical and Physical Character*, 115(772):700–721, 1927.
- 16 Lauri Kovanen, Márton Karsai, Kimmo Kaski, János Kertész, and Jari Saramäki. Temporal motifs in time-dependent networks. *Journal of Statistical Mechanics: Theory and Experiment*, 2011(11):P11005, 2011. doi:10.1088/1742-5468/2011/11/P11005.
- 17 Audun Myers, David Munoz, Firas A Khasawneh, and Elizabeth Munch. Temporal network analysis using zigzag persistence. *EPJ Data Science*, 12:45, 2023.
- 18 Lutz Oettershagen, Nils M. Kriege, Christopher Morris, and Petra Mutzel. *Temporal Graph Kernels for Classifying Dissemination Processes*. 2020.

- 19 Ashwin Paranjape, Austin R Benson, and Jure Leskovec. Motifs in temporal networks. *Proceedings of the Tenth ACM International Conference on Web Search and Data Mining*, 2017.
- 20 Jan Reininghaus, Stefan Huber, Ulrich Bauer, and Roland Kwitt. A stable multi-scale kernel for topological machine learning. In *IEEE Conference on Computer Vision and Pattern Recognition (CVPR)*, pages 4741–4748, 2015.
- 21 Emanuele Rossi, Ben Chamberlain, Fabrizio Frasca, Davide Eynard, Federico Monti, and Michael M. Bronstein. Temporal graph networks for deep learning on dynamic graphs. In *Proceedings of the International Conference on Learning Representations (ICLR) Workshop*, 2020.
- 22 Koya Sato, Mizuki Oka, Alain Barrat, and Ciro Cattuto. Dyane: Dynamics-aware node embedding for temporal networks. *arXiv preprint arXiv:1909.05976*, 2019.
- 23 Till Schulz, Pascal Welke, and Stefan Wrobel. Graph filtration kernels. volume 36, 2022.
- 24 Bernhard Schölkopf and Alexander J. Smola. *Learning with Kernels: Support Vector Machines, Regularization, Optimization, and Beyond*. MIT Press, Cambridge, MA, 2002.
- 25 Kiarash Shamsi, Farimah Poursafaei, Shenyang Huang, Bao Tran Gia Ngo, Baris Coskunuzer, and Cuneyt Gurcan Akcora. Graphpulse: Topological representations for temporal graph property prediction. In *The Twelfth International Conference on Learning Representations*, 2024. URL: <https://openreview.net/forum?id=DZqic2sPTY>.
- 26 Nino Shervashidze, Pascal Schweitzer, Erik Jan van Leeuwen, Kurt Mehlhorn, and Karsten M. Borgwardt. Weisfeiler-lehman graph kernels. *Journal of Machine Learning Research*, 12:2539–2561, 2011.
- 27 Arkadiusz Stopczynski, Vedran Sekara, Piotr Sapiezynski, Andrea Cuttone, Mikko M. Madsen, and Sune Lehmann. Measuring large-scale social networks with high resolution. *PLoS ONE*, 2014.
- 28 Raphaël Tinarrage, Jean R. Ponciano, Claudio D. G. Linhares, Agma J. M. Traina, and Jorge Poco. Tdanetvis: Suggesting temporal resolutions for graph visualization using zigzag persistent homology. 2023. URL: <https://arxiv.org/abs/2304.03828>, arXiv:2304.03828.
- 29 Kun Tu, Jian Li, Don Towsley, Dave Braines, and Liam D. Turner. Network classification in temporal networks using motifs. 2018. URL: <https://arxiv.org/abs/1807.03733>, arXiv:1807.03733.
- 30 Haishuai Wang. Time-variant graph classification. 2017. URL: <https://arxiv.org/abs/1609.04350>, arXiv:1609.04350.
- 31 Haishuai Wang, Jia Wu, Xingquan Zhu, Yixin Chen, and Chengqi Zhang. Time-variant graph classification. *IEEE Transactions on Systems, Man, and Cybernetics: Systems*, 50(8):2883–2896, 2020. doi:10.1109/TSMC.2018.2830792.
- 32 Boris Weisfeiler and Andrei A. Leman. The reduction of a graph to canonical form and the algebra which appears therein. *NTI, Series 2*, 9:12–16, 1968.
- 33 Dongsheng Ye, Hao Jiang, Ying Jiang, and Hao Li. Stable distance of persistent homology for dynamic graph comparison. *Knowledge-Based Systems*, 278:110855, 07 2023. doi:10.1016/j.knosys.2023.110855.
- 34 Afra Zomorodian and Gunnar Carlsson. Computing persistent homology. *Discrete & Computational Geometry*, 33(2):249–274, 2005.